Far-Field Prediction using only Magnetic Near-Field Scanning for EMI Test

Xu Gao, *Student Member, IEEE,* Jun Fan, *Senior Member, IEEE,* Yaojiang Zhang, *Senior Member, IEEE,* Hamed Kajbaf, *Member, IEEE,* and David Pommerenke, *Senior Member, IEEE*

***Abstract*—Far-field prediction for EMI testing was achieved using only magnetic near-field on a Huygens surface. The electrical field on the Huygens surface was calculated from the magnetic near-field using the finite element method (FEM). Two examples were used to verify the proposed method. The first example used the field radiated by an infinitesimal electric dipole. The calculated results were compared with the analytical solution. In the second example, the calculated results were compared with full-wave simulation results for the radiation of a print circuit board (PCB). The validity of this method when the near-field is high-impedance field was verified as well. Sensitivity of the far-field to noise in both magnitude and phase in the near-field data was also investigated. The results indicate that the proposed method is very robust to the random variation of both. The effect of using only four sides of the Huygens box was investigated as well, revealing that, in some instances, the incomplete Huygens's box can be used to predict the far-field well. The proposed method was validated using near-field measurement data taken from a sleeve dipole antenna. The error for the maximum far field value was in only 1.3 dB.**

***Index Terms*—Near-field far-field transformation, Equivalence theorem, Magnetic fields, Finite element methods, Electromagnetic interference.**

I. Introduction

NEAR-FIELD scanning has been used extensively for the far-field estimation of antennas [1]-[5]. Applied to electromagnetic compatibility (EMC) problems, near-field scanning has been used to estimate emissions from both integrated circuits (ICs) and printed circuit boards (PCBs) [6]-[13]. Interest in applying far-field predictions using near-field to EMI/EMC problems has recently grown. To predict the far-field emissions from a PCB in the top half space, the near-field data on a planar surface above PCB usually is sufficient [6][7][8]. However, near-field measurement on only one planar surface may not be enough to predict the far-field radiation of three-dimensional structures. The near-field on an enclosed Huygens's surface may be preferred for near-field scanning when predicting the far-field radiation associated with the EMI problems of some complex structures.

Two principle approaches are typically used for near-field far-field transformation. One method relies on expanding the field by a superposition of modes [14]. The other is based on equivalent electric current sources [1][7] and/or equivalent magnetic current sources [2]. In [1], only the equivalent electric current is used for the near-field far-field transformation using a horn antenna as an example. The electric current is obtained from the magnetic near-field on the planar surface at outlet of a horn. In this case, the electric near-field is not needed due to two reasons. The first reason is that the equivalence principle [19](also described in Section II.) is applied here. The second one is that the image theory for infinite-large planar perfect magnetic conductor (PMC) boundary is also used. Similar reasoning was applied in [2]. The authors of [7], use a planar surface of equivalent sources above PCB to predict the far-field emission from the PCB. Image theory allows to use only one class of equivalent sources. However, the usage of only one type of equivalent sources combined with image theory requires a large planar Huygens's surface that covers area beyond the PCB size. The planar Huygens's surface is usually used to calculate far-field in half space above the surface. For more general cases, for example, a Huygens's box enclosing all sources, the simplification resulting from applying image theory cannot be used, because image theory can be only used for either infinite-large perfect electric conductor (PEC) plane or infinite-large PMC plane. Thus, both equivalent electric current obtained from the tangential magnetic field and equivalent magnetic current obtained from the tangential electric field are needed to perform far-field transformation from near-field data [19].

Designing electric field probes for tangential components is more difficult than designing magnetic field probes. As a result and in the interest of reducing scan time, far-field transformation based only on magnetic field near-field measurements is preferred. Since electric near-field is required to calculate the far field, methods to extracted electric field from magnetic field were proposed in [15][16] based on the principle of plan wave spectrum. However, the method discussed in [15][16] is constrained to planar near-field scanning and cannot be used on an arbitrarily shaped Huygens's surface. In [4], a good method is proposed to reconstruct equivalent currents on arbitrary three dimensional Huygens's surface based on the integral equation algorithms and the Conjugated Gradient (CG) method.

This paper proposes a novel method to extract the electric field from the tangential magnetic field on an arbitrary shaped Huygens's surface. It does not rely on image theory. For EMC applications the near field is used to predict the maximum

Manuscript received June 18, 2013. This work was supported in part by the National Science Foundation (NSF) under Grant 0855878.

far-field. The robustness of the method against input data errors is investigated and shown using measured data.

Several practical issues need to be considered for near-field scanning to be successful. Due to obstruction by structures that hold the DUT, and a limited ability to robotically place the probe at any location in the desired tangential orientation it is difficult to obtain near-field data on all sides of a 6-sided Huygens box. The effect of incompleteness of Huygens's surface is investigated in this paper. These results indicate that the maximum of the far-field, radiated to the side of the Huygens's box can still be retrieved if the bottom and the top surfaces are missing. The effect of measurement inaccuracy on the far-field is also investigated.

This paper is organized into seven sections. The theoretical basis and procedure of the proposed method are described in Section II and Section III, respectively. Two examples are used in Section IV to verify the proposed method. In Section V, both the effect of inaccuracy of magnetic near-field and the effect of using incomplete Huygens's box on the far-field result are investigated. In Section VI, the proposed method is validated using real near-field scanning data for a sleeve dipole. Final, discussions and conclusions are reported in Section VII.

II. Brief Review of Theory

The equivalence theorem (Huygens's principle) is well known and widely used in the electromagnetic area [19]. Fig. 1 depicts the equivalence theorem. The actual radiating sources ($J1$ and $M1$) are enclosed inside surface S, as shown in Fig. 1 (a). If the electromagnetic field outside the enclosed surface S is the only field of interest, one can substitute the sources with equivalent electric and magnetic currents placed on the surface of S, as shown in Fig. 1 (b). Love's equivalence principle is used to move from the situation in Fig.1 (a) to the situation in Fig. 1 (b). The fields within the surface S are set to zeros, and the equivalent sources become:

$$\overline{J_s} = \hat{n} \times \overline{H_2}\big|_S \tag{1}$$

$$\overline{M_s} = -\hat{n} \times \overline{E_2}\big|_S \tag{2}$$

Based on the equivalent problem shown in Fig. 1 (b), the fields $\overline{E_2}$ and $\overline{H_2}$ outside the surface S can be determined by using (3-6).

$$\overline{A} = \frac{\mu}{4\pi} \iint_s \overline{J_s} \frac{e^{-j\beta R}}{R} ds' \tag{3}$$

$$\overline{F} = \frac{\varepsilon}{4\pi} \iint_s \overline{M_s} \frac{e^{-j\beta R}}{R} ds' \tag{4}$$

$$\overline{E} = -j\omega\overline{A} - j\frac{1}{\omega\mu\varepsilon}\nabla(\nabla\cdot\overline{A}) - \frac{1}{\varepsilon}\nabla\times\overline{F} \tag{5}$$

$$\overline{H} = \frac{1}{\mu}\nabla\times\overline{A} - j\omega\overline{F} - j\frac{1}{\omega\mu\varepsilon}\nabla(\nabla\cdot\overline{F}) \tag{6}$$

where $R = |\bar{r} - \bar{r}'|$, $\bar{r}$ is the observation point, and $\bar{r}'$ is the source point.

In the equivalent problem given in Fig. 1 (b), both the tangential magnetic field and the electric fields on the surface S are used to establish the equivalent source. However, based on the electromagnetic uniqueness theorem, the tangential components of only magnetic or electric field on surface S is needed to determine the field outside surface S. This allows considering the problem as show in Fig. 1 (c). Because both the E and the H field are zero within the surface S, fields cannot be disturbed if the properties of the medium within S are changed.

A further simplification can be obtained by filling the volume V1 with perfect magnetic material (PMC). The PMC boundary prohibits the radiation from the equivalent magnetic current source [19]. The equivalent magnetic current is considered to be zero. In this case, only the tangential magnetic field is used to determine all equivalent sources. The equivalent problem translates to the radiation of electric current sources on a PMC boundary. The advantage of this equivalence is that only the tangential magnetic field on the surface S is needed, but the difficulty of it is that (3-6) cannot be used anymore, because the current sources do not radiate into unbounded medium.

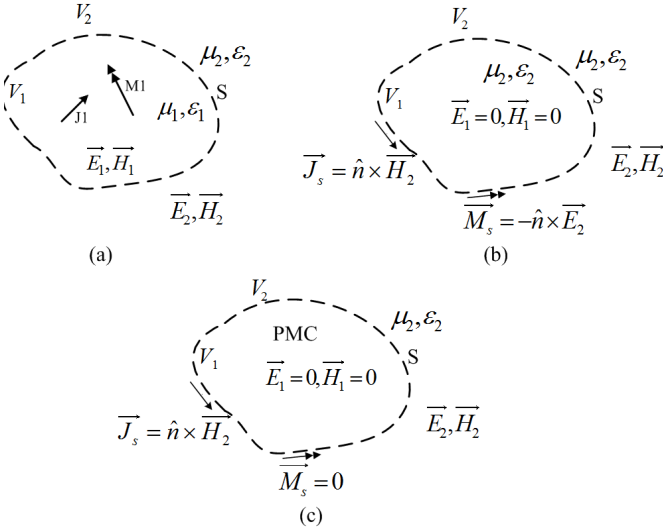

Fig. 1. Equivalence principle models. (a) Original problem. (b) Love's equivalent problem. (c) Equivalent problem when PMC is filled.

In the EMC testing, the equivalence principle could be used to predict the far-field radiation from near-field scanning. However, to perform the near-field-far-field transformation using the equivalence in Fig. 1 (b), the tangential components of both electric and magnetic fields on the complete Huygens's surface are needed theoretically. As previously mentioned, fabricating an electric field probe for the tangential field is relatively difficult. Consequently, a method that uses only magnetic fields would be helpful.

In real near-field scanning, several types of geometries are used as an enclosed Huygens's surface (i.e., sphere and box). The rectangle Huygens's box is used in this paper. However, the proposed method is not only suitable for the rectangle Huygens's box, but also for other geometries.

III. Description of The Proposed Method

Fig. 2 illustrates the main steps of the method. The method starts with having only the tangential's magnetic field in phase and magnitude for six sides as input data. As the method used

for the phase measurement is not relevant to the post processing, different phase measurement techniques can be applied [7][17][18][22]. The middle box shows the method to retrieve the missing tangential electric field. The tangential magnetic field, converted into equivalent electric currents, is applied as excitation on a PMC box. This is solved by finite element method (FEM) [20]. The FEM calculation determines the missing tangential electric field. After the tangential electric field is obtained Huygens's principle (Fig. 1(b)) is used to determine the far field using equations (3-6) which have been implemented based on [4][19]. Fig. 2(b) gives a flow diagram of the proposed method. The setup of FEM implementation is shown in Fig. 3.

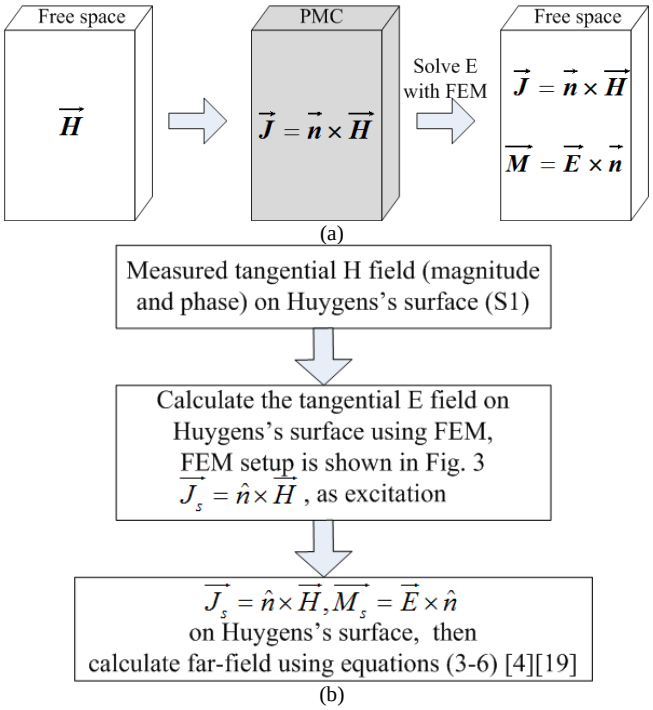

Fig. 2. Procedure of the proposed method. (a) The left box shows the original problem. The middle box shows the equivalent problem. FEM was used to solve the equivalent problem to obtain the tangential electric on the surface of the Huygens's box. The right box shows the equivalence to calculate the far-field. (b) The flow diagram of the proposed method.

The equivalent electric current sources were determined using (1). The PMC boundary condition was then assigned to the surface of the Huygens's box (the surface S1in Fig. 3). A larger radiation box was implemented outside the Huygens's box to terminate the FEM domain. Here, the absorbing boundary conditions were implemented on the inside surface (S2) of the radiation box. The volume between surfaces S1 and S2 was the calculation region. This region needed to be meshed. The wave equation in (7) was solved using FEM to obtain the tangential electric field on the surface S1.

$$\nabla \times \left(\frac{1}{\mu_r} \nabla \times \vec{E} \right) - k_0^2 \varepsilon_r \vec{E} = -jk_0 Z_0 \vec{J} \qquad (7)$$

where k_0 is the free-space wave number and Z_0 is the wave impedance in free space.

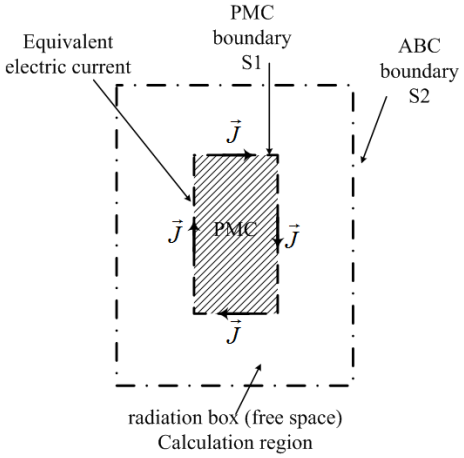

Fig. 3. FEM implementation for determining the electric field on the Huygens's box.

IV. Verification of the Proposed Method

A. Example using an infinitesimal dipole

For simplicity, the first example used to test the proposed method was an infinitesimal electric dipole along the z-direction, as shown in Fig. 4. This dipole was placed at the center of the Huygens's box. The magnetic field on the surface of the Huygens's box was obtained from the analytical solution of the fields for a dipole. The electric field was then calculated using the proposed method. The calculated electric field was compared with the analytical solution. Finally, the far field was determined using (1-6). These results were compared to the analytical solution for the far-field of an infinitesimal dipole. Since there are six faces in the Huygens's box, for clarity, in the following text, face z1 and face z2 denotes the two faces perpendicular to z-axis, and the z-coordinates of face z2 is larger than that of face z1. For example, in Fig. 4, face z1 is the bottom face of the Huygens's box. Face z2 is the top face. The similar meaning for face x1 and face x2, face y1 and face y2 was used in the following text.

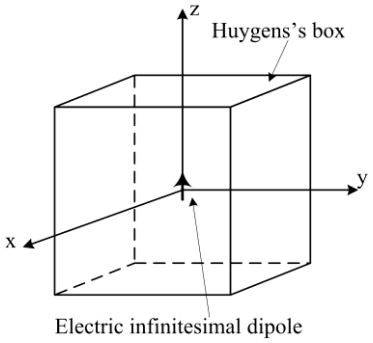

Fig. 4. A test example using an infinitesimal electric dipole

The dimension of the Huygens's box shown in Fig. 4 was 100×100×100 mm; 500 MHz was selected as the test frequency. The equivalent electric currents on the surface of the Huygens's surface were obtained analytically. These currents were used as sources to calculate the electric field on the surface of the Huygens's box. A FEM solver implemented in Matlab was used to calculate the electric field. The calculated tangential electric fields on face x2 are given in Fig. 5. These fields were compared with the analytical solution. The

comparison of electric fields on other faces reveals a similar behavior. Both the calculated results agree well with the analytical results. Although some numerical noise was present in the calculated results, these noises had little effect on the accuracy of the far field calculation.

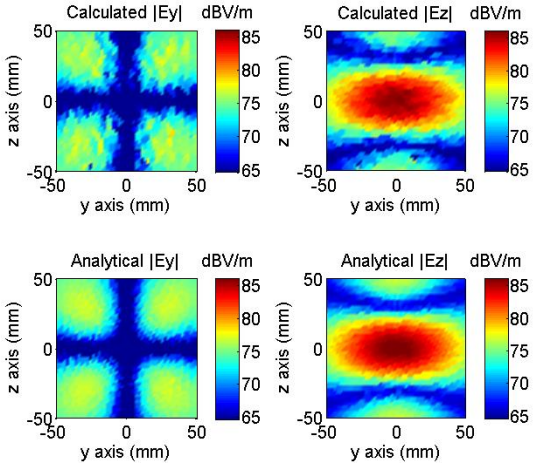

Fig. 5. Comparison of calculated and analytical electric field on the surface of Huygens's box: face x2.

Fig.6 shows the far-field calculation result on the XZ plane. This far-filed was calculated using (1-6) with the calculated electric field. This result were compared the analytical results. The Root Mean Square (RMS) error was less than 0.01, providing evidence that the proposed method was correctly implemented. Next, the same method was applied to a PCB, mounted on a metallic box, without symmetry.

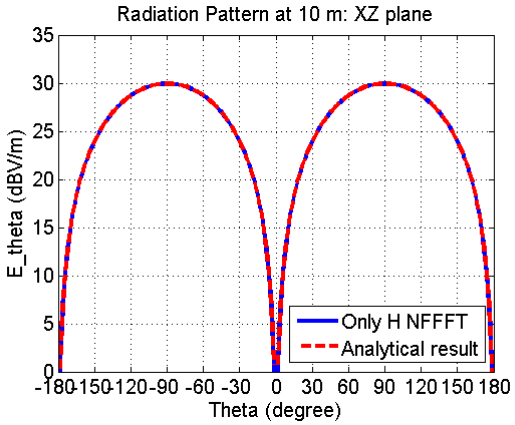

Fig. 6. Comparison of calculated electric field radiation pattern with analytical result on the XZ cutting-plane.

B. *Example of a PCB board on a metal box*

The geometry, shown in Fig. 7, consisted of a 50 Ω load terminated trace with a patch added to it. The Huygens's box has a distance of 2 cm to the box. The dimensions of the Huygens's box were 80×50×130 mm. 500 MHz was again selected as the test frequency. A references solution was obtained using EMC-Studio [21]. The simulated magnetic field on the Huygens's box was exported from EMC-Studio and used as input for the proposed method. For the compactness of the paper, only the final far-field calculation results are presented here. Fig. 8 compares the far-field at 3 m in the XY plane. The calculated results (using the proposed method) closely matched the simulation results. The RMS errors were 0.02 and 0.01 for theta component and phi component, respectively.

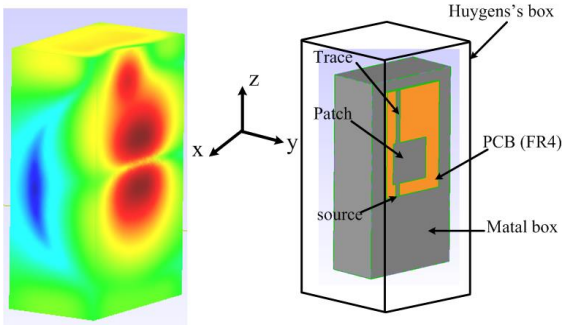

Fig. 7. Simulation model in EMC studio.

The situation in which the electric field dominates in near-field must be investigated, because the proposed method use only magnetic field on Huygens's box. In that situation, the field impedance on Huygens's surface was higher than the wave impedance in air (377 Ω). Thus, the same PCB example without termination at the end of the trace was tested at 50 MHz. The field impedance in near-field in this situation was high, due to the open end of trace and the low frequency. Fig. 9 is a histogram of the field impedance at the sampling points on face y2 for two cases. Fig.9 (a) is the case at 500 MHz with termination and Fig. 9 (b) is the case at 50 MHz without termination. These histograms clearly show that, for the case at 50 MHz without termination, the average field impedance on Huygens's box was much higher than 377 Ω.

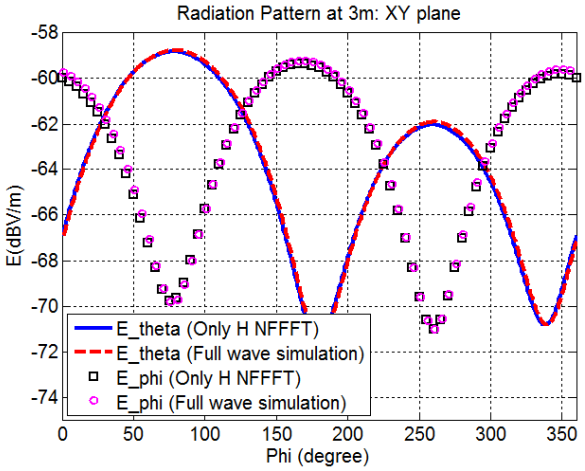

Fig. 8. Comparison of the calculated far-field results of the PCB example using the proposed method with the full wave simulation results at 500 MHz, E_theta and E_phi in XY plane.

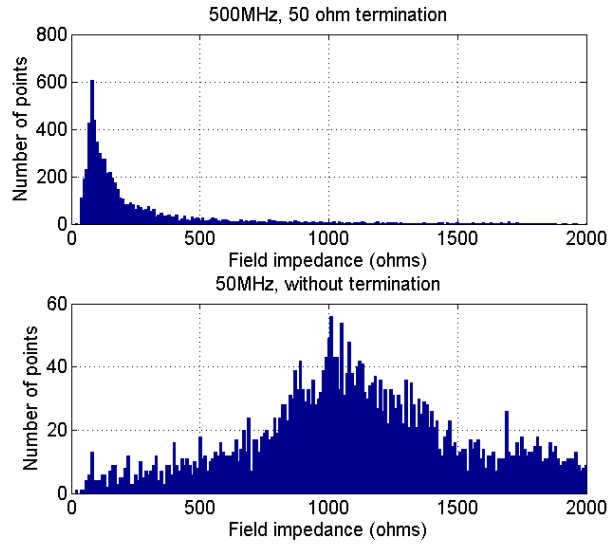

Fig. 9. Histogram for field impedance on face y2. (a) 500 MHz with termination. (b) 50 MHz without termination.

Fig. 10 shows the far-field calculation for the second case. Again, the proposed method worked very well, indicating that it can be used for the case with high field impedance in near-field.

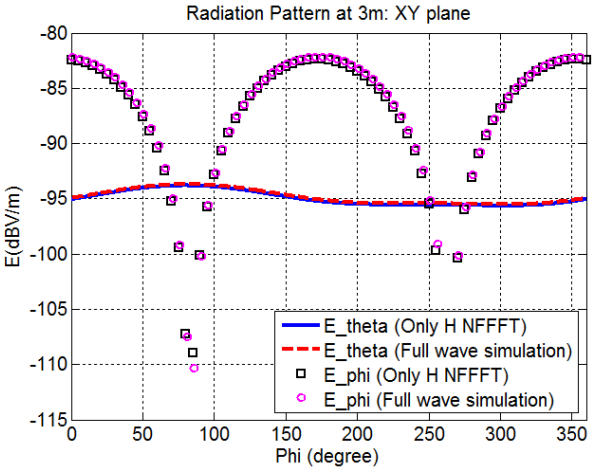

Fig. 10. Calculation results of far-field at 50 MHz for the case without termination, E_theta and E_phi in XY plane.

V. Investigation on Issues in Practical Scanning

Near-field scanning results are affected by thermal noise, positioning errors, the coupling of insufficiently suppressed field components, phase measurement errors and amplitude measurement errors. In this section, inaccuracies were introduced to the magnetic field to investigate the propagation of noise from the initial magnetic field to the far field result. The same PCB board example at 500 MHz was used in this section.

A. Magnitude error in scanning magnetic field

The randomly distributed magnitude error was added to the simulated magnetic field on the Huygens's box to investigate the noise effect on the proposed method. The amplitude of the noise was +/- 5 dB. This value means the magnetic field strength varied by multiplying factors. These factors were randomly distributed between 0.6 and 1.8. Fig. 11 illustrates the equivalent electric current. This current was obtained from the magnetic field using (1), both with and without the magnitude noise on face y2. The magnitude error was added for all faces of the Huygens's box. Here, only the z component of the equivalent electric current on face y2 is shown. The other faces show similar behavior.

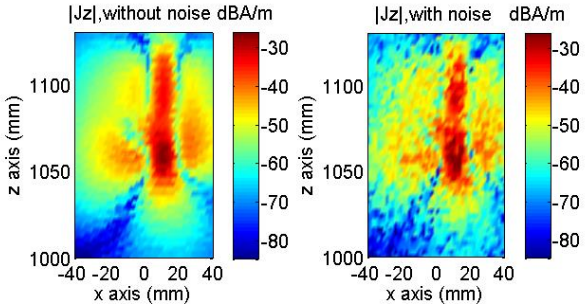

Fig. 11. The equivalent electric currents, both with and without magnitude noise, on face y2. The amplitude of noise is +/- 5 dB and randomly distributed.

The resulting far-field is illustrated in Fig. 12. Although the noise has some effects on the calculated results, these results still agree with the simulation results using the full wave simulation tool. EMI testing is primarily focused on the maximal field. Here, the differences between the calculated maximal E-field and the maximal E-field of full wave simulation are 1.2 dB and 0.1 dB for vertical polarization and horizontal polarization, respectively. This suggests that the proposed method is relatively robust to randomly distributed magnitude noise typically present in scanned near-field data.

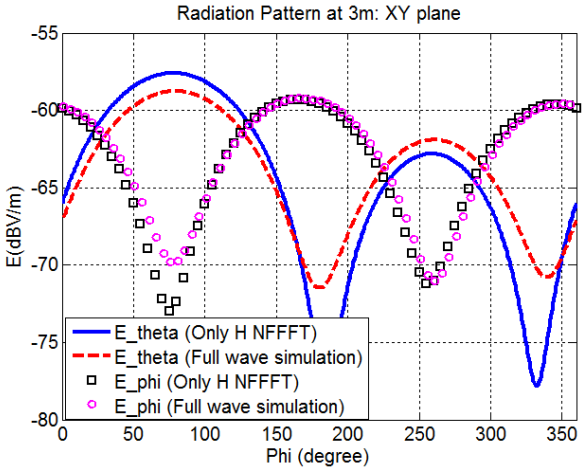

Fig. 12. The effect of magnitude error (+/- 5 dB) in the scanning H field to the far-field results, E_theta and E_phi in XY plane.

B. Random variations in the phase of scanning magnetic field

A random phase deviation of +/- 30 degree was introduced to investigate the effect of random deviations of the phase from the real phase value, as shown in Fig. 13. Again, only the phase of equivalent electric current on face y2 is presented. For other faces, the effect of the random phase noise on the equivalent current was similar.

The far-field results (illustrated in Fig. 14) indicate that the random phase variations of the magnetic field did not greatly affect the final far-field calculation results. For the maximum electric field, the differences between the calculated results and

full wave simulation result are 0.9 dB and 0.2 dB for vertical polarization and horizontal polarization, respectively. This suggests that the proposed method is also relatively robust to randomly distributed phase deviations typically present in scanned near-field data.

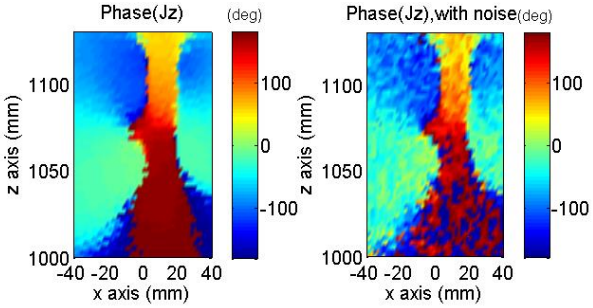

Fig. 13. The equivalent electric currents, both with and without phase variation, on face y2. The amplitude of noise was +/- 30 degree and randomly distributed.

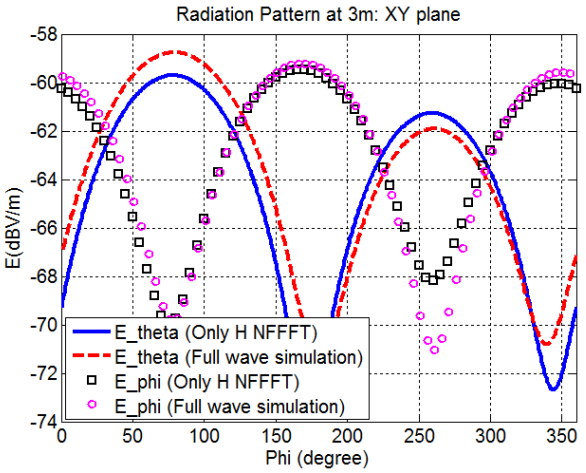

Fig. 14. The effect of phase variation (+/- 30 degree) in the scanning H field on the far-field results using the proposed method, E_theta and E_phi in XY plane.

C. Calibration error

Uncertainties in the probe calibration can lead to errors in the near field data. As long as the probe calibration error is not a function of the probe location during scanning, a linear relationship exits between the probe calibration error and the resulting error in the far field. This fact is illustrated in Fig. 15, a 3dB error was observed in the far-field resulted as a result of a 3dB error in the input H-field data. This linear relationship is mainly due to the linear property of FEM method.

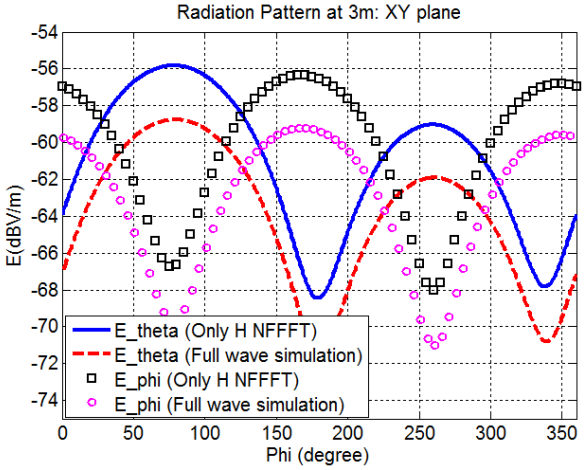

Fig. 15. The effect of 3 dB calibration error in H-field on the far-field results using the proposed method, E_theta and E_phi in XY plane.

D. Incomplete Huygens's box

In real near-field scanning, measuring the magnetic field on all of the faces of the Huygens's box may be difficult. This difficulty may be due to DUT holders and limited reach of the robotic scanner. The effect of incomplete Huygens's boxes on the far-field was investigated therefore. The main radiation of the PCB example board was in the XY plane. The far-field was also analyzed in the XY plane. The magnetic fields on face z1 and face z2 were assumed unknown and set to zero in the proposed method. In this calculation, only magnetic fields on the four side faces (face x1, face x2, face y1 and face y2) were used, which means an incomplete Huygens's box is used. The far-field calculation results using the proposed method are presented in Fig. 16. Although the incompleteness of the Huygens's box slightly deteriorates the far-field calculation results, the error is small. For the maximum E field, the differences between the calculated results and the full wave simulation results are 0.3 dB and 2.6 dB for vertical polarization and horizontal polarization, respectively. This test result confirms that neither the top surface nor the bottom surface of the Huygens's box contribute significantly to the far-field in XY plane, in which the main radiation direction is included, so they can be set to zeros. Of course, the top and bottom surfaces of the Huygens's box will have an effect on the far field in the top and bottom direction, however, in this PCB example, they are not main radiating directions.

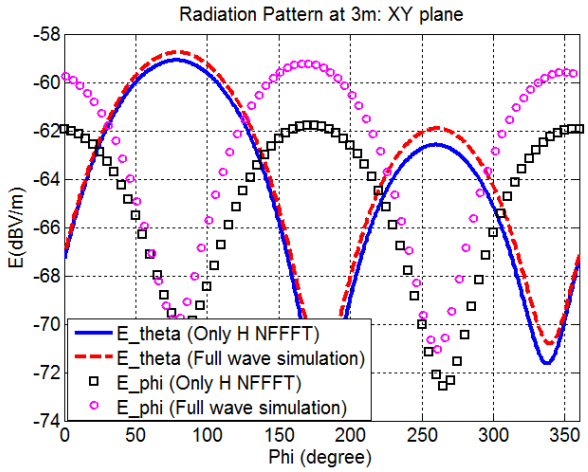

Fig. 16. The effect of incompleteness of Huygens's box on the far-field results using the proposed method, E_theta and E_phi in XY plane.

VI. Measurement Validation

A 922 MHz sleeve dipole antenna was constructed to test the performance of the proposed method. The magnetic field was measured. Fig. 17(a) shows the measurement setup. An oscilloscope measured both the magnitude and the phase of magnetic fields. The phase information was obtained by comparing the measured signal and the reference signal. The characteristics of the amplifier and cable were calibrated using a network analyzer. A 5-mm H-field probe was used. The calibration method is described in [22]. Due to the rotational symmetry of the antenna, only the magnetic near-field on face x2 was scanned using API 3D scanning system. The magnetic fields on the bottom face were not scanned because of the feeding cable. The fields on the top face were omitted as well. The calculation was based on both one measured side face and the assumption of symmetry. The length of the dipole antenna was 150 mm. The dimension of the scanning area (on face x2) was 80×190 mm, and the scanning face was 20 mm away from the sleeve dipole antenna. Fig. 18 illustrates the measured equivalent electric current on face x2 after conversion from the measured magnetic field. Theoretically, for dipole, the y-component of the equivalent electric current should be zero, however in real measurement it is not zero due to the non-ideal fabrication of dipole and probe coupling. The ratio of the magnitude of J_z to the magnitude of J_y is also shown in Fig. 18 to give feeling of the rejection to J_y in measurement.

The calculated electric field in the X-Z cutting plane is shown in Fig. 19. The calculation result was compared with analytical result for the dipole antenna. The maximal far-field was calculated and compared with the same input power applied during measurement (see Table I). A good agreement was obtained for the maximum electric field. The difference was only 1.3 dB. The incomplete Huygens's box was used for the sleeve dipole antenna, because in this case the contribution of the equivalent sources on the top and bottom faces to the far-field radiating field are not important compared with that on other faces.

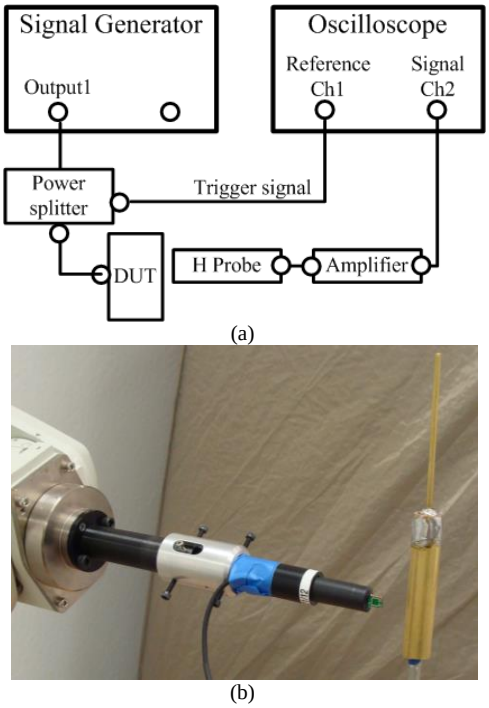

Fig. 17. Near-field scanning for a sleeve dipole antenna. (a) Measurement Setup. (b) photograph of probe and DUT.

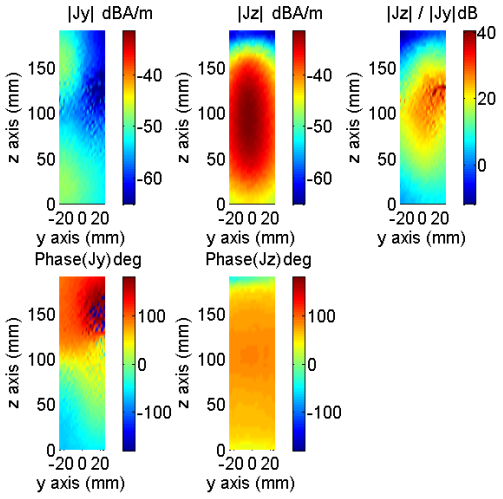

Fig. 18. The measured equivalent electric current of the sleeve dipole on face x2 of the Huygens's box

TABLE I

	Only H NFFFT	Analytical solution
Maximum E field at 10 m (dBV/m)	-33.2	-31.9

The comparison of the calculated result using the proposed method and the analytical result for the maximum E field

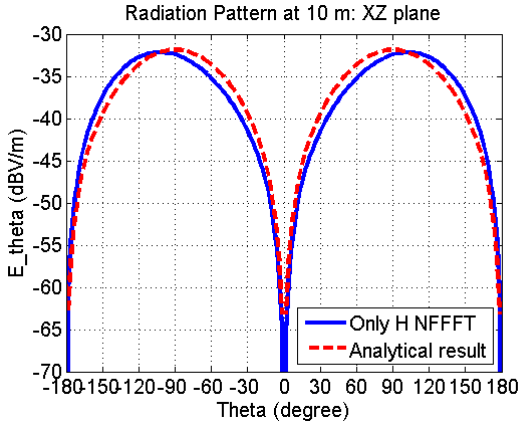

Fig. 19. Calculated electric field radiation pattern of the sleeve dipole using the proposed method. Comparison with analytical result on XZ cutting-plane.

VII. Discussions and Conclusions

When using a Huygens's box, both the tangential electric and the magnetic field are needed. In this paper, a novel method is proposed to predict the far-field radiation using only the magnetic near-field component on a Huygens's box. The proposed method was verified with two simulated examples and one measurement case. The effect of inaccuracy of magnetic field and the incompleteness of the Huygens's box on far-field results is investigated in this paper. The proposed method can be applied for arbitrary shapes of closed Huygens's surfaces. Only the tangential magnetic field needs to be measured. And it also shows good accuracy and robustness in use. Measuring only the magnetic field cuts the scan time in half. However, there are also several limitations or disadvantage with this method. At first, the proposed method needs to measure a closed Huygens's surface. In some cases, measuring on a close surface may be difficult. This difficulty may be due to DUT holders and limited reach of the robotic scanner. Therefore as shown in this paper, in some cases, an incomplete Huygens's box can be also used for the proposed method. However, if lots of energy goes through the eliminated side, this method will fail probably. Secondly, the proposed method is a narrow-band method because that FEM is frequency-domain method, while wide-band method is preferred for EMI/EMC application. However, this problem can be mitigated by dividing the wide-band into several smaller bands.

References

[1] T.K. Sarkar, A. Taaghol, "Near-field to near/far-field transformation for arbitrary near-field geometry utilizing an equivalent electric current and MoM," *Antennas and Propagation, IEEE Transactions on*, vol.47, no.3, pp.566-573, Mar 1999.

[2] P. Petre, T.K. Sarkar, "Planar near-field to far-field transformation using an equivalent magnetic current approach," Antennas and Propagation, IEEE Transactions on , vol.40, no.11, pp.1348-1356, Nov 1992.

[3] A. D. Yaghjian, "An Overview of Near-field Antenna Measurements" *Antennas and Propagation, IEEE Transactions on*, Vol. AP- 34, No. 1, 1986.

[4] Y. Alvarez, F. Las-Heras, M.R. Pino, "Reconstruction of Equivalent Currents Distribution Over Arbitrary Three-Dimensional Surfaces Based on Integral Equation Algorithms," *Antennas and Propagation, IEEE Transactions on* , vol.55, no.12, pp.3460-3468, Dec. 2007

[5] C.H. Schmidt, M.M. Leibfritz, T.F. Eibert, "Fully Probe-Corrected Near-Field Far-Field Transformation Employing Plane Wave Expansion and Diagonal Translation Operators," *Antennas and Propagation, IEEE Transactions on* , vol.56, no.3, pp.737-746, March 2008

[6] M. M. Hernando, A. Fernández, M. Arias, M. Rodríguez, Y. Álvarez, F. Las-Heras, "EMI radiated noise measurement system using the source reconstruction technique," *IEEE T. on Industrial Electronics*, vol. 55, no. 9, September 2008.

[7] Y. Álvarez, M. Rodríguez, F. Las-Heras, M. M. Hernando, "On the use of the source reconstruction method for estimating radiated EMI in electronic circuits," *IEEE T. on Instrumentation and Measurement*, vol. 59, no. 12, December 2010.

[8] M. Hernando, A. Fernandez, M. Arias, M. Rodriguez, Y. Alvarez, F. Las-Heras, "Radiated noise measurement system to estimate the EMI regulations compliance of a power electronic circuit," *Industrial Electronics, 2007. ISIE 2007. IEEE International Symposium on* , vol., no., pp.2544,2549, 4-7 June 2007.

[9] Haixiao Weng, D.G. Beetner, R.E. DuBroff , "Prediction of Radiated Emissions Using Near-Field Measurements," *Electromagnetic Compatibility, IEEE Transactions on* , vol.53, no.4, pp.891-899, Nov. 2011

[10] Z. Yu, J. A. Mix, S. Sajuyigbe, K. P. Slattery, J. Fan, "An Improved Dipole-Moment Model Based on Near-Field Scanning for Characterizing Near-Field Coupling and Far-Field Radiation From an IC," *Electromagnetic Compatibility, IEEE Transactions on* , vol.55, no.1, pp.97-108, Feb. 2013

[11] Z. Yu, J. A. Mix, S. Sajuyigbe, K. P. Slattery, D. Pommerenke, J. Fan, "Heat-Sink Modeling and Design With Dipole Moments Representing IC Excitation," *Electromagnetic Compatibility, IEEE Transactions on* , vol.55, no.1, pp.168-174, Feb. 2013

[12] B. Deutschmann, H. Pitsch, and G. Langer, "Near field measurements to predict the electromagnetic emission of integrated circuits," in *Proc. 5th Int. Workshop Electromagn. Compat. Integr. Circuits*, Munich, Germany, Nov. 28–30, 2005, pp. 27–32.

[13] J. Shi, M. A. Cracraft, J. ZhangM., R. E. DuBroff, and K. Slattery, "Using near-field scanning to predict radiated fields," in *Proc. IEEE Int. Symp. Electromagn. Compat.*, Santa Clara, CA, Aug. 2004, pp. 14–18.

[14] J. E. Hansen et al., Spherical Near-Field Antenna Measurements, ser. IEE Electromagnetic Waves Series. London, U.K.: Peter Peregrinus, 1988, vol. 26.

[15] Y. Liu, B. Ravelo, A.K. Jastrzebski, J. Ben Hadj Slama, "Computational method of extraction of the 3D E-field from the 2D H-near-field using PWS transform," *EMC Europe 2011 York* , vol., no., pp.555-560, 26-30 Sept. 2011

[16] Liu Yang, B. Ravelo, A.K. Jastrzebski, "Calculation of time-domain near-field Ex, y, z(t) from Hx, y(t) with PWS and FFT transforms," *Electromagnetic Compatibility (EMC EUROPE), 2012 International Symposium on* , vol., no., pp.1-6, 17-21 Sept. 2012

[17] Y. Vives-Gilabert, C. Arcambal, A. Louis, F. De Daran, P. Eudeline, B. Mazari, "Modeling Magnetic Radiations of Electronic Circuits Using Near-Field Scanning Method," *Electromagnetic Compatibility, IEEE Transactions on* , vol.49, no.2, pp.391,400, May 2007.

[18] Weng Haixiao, D.G. Beetner, R.E. DuBroff, Shi Jin, "Estimation of High-Frequency Currents From Near-Field Scan Measurements," *Electromagnetic Compatibility, IEEE Transactions on* , vol.49, no.4, pp.805,815, Nov. 2007.

[19] C. A. Balanis, *Advanced Engineering Electromagnetics*. New York: Wiley, 1989.

[20] Jian-Ming Jin. *The finite element method in electromagnetics*. New York: Wiley, 1993.

[21] http://www.emcos.com/EMC.

[22] J. Zhang, K. Kam, Jin Min; V. Khilkevich, D. Pommerenke, Jun Fan, "An Effective Method of Probe Calibration in Phase-Resolved Near-Field Scanning for EMI Application," *Instrumentation and Measurement, IEEE Transactions on* , vol.62, no.3, pp.648,658, March 2013